Calibration-Free Image-Based Trajectory Tracking Control of Mobile Robots With an Overhead Camera

Xinwu Liang, *Member, IEEE*, Hesheng Wang, *Senior Member, IEEE*, Yun-Hui Liu, *Fellow, IEEE*, Bing You, Zhe Liu, and Weidong Chen, *Member, IEEE*

***Abstract*— To make the controller implementation easier and to enhance the system robustness and control performance in the presence of the camera parameter uncertainties, it is very desired to develop vision-based control approaches without any offline or online camera calibration. In this article, we propose a new calibration-free image-based trajectory tracking control scheme for nonholonomic mobile robots with a truly uncalibrated fixed camera. By developing a novel camera-parameter-independent kinematic model, both offline and online camera calibration can be avoided in the proposed scheme, and any knowledge of the camera is not needed in the controller design. The proposed trajectory tracking control scheme can guarantee exponential convergence of the image position and velocity tracking errors. To illustrate the performance of the proposed scheme, experimental results are provided in this article.**

***Note to Practitioners*—This article was motivated by the vision-based motion control problem of mobile robots in uncalibrated environments. Existing vision-based motion control approaches for nonholonomic mobile robots generally depend on offline precise/coarse or online numerical/adaptive calibration of the camera intrinsic and extrinsic parameters and require precise or coarse knowledge of the camera in their implementation. This article presents a novel calibration-free image-based trajectory tracking control scheme, which can be implemented easily in real environments without any offline or online calibration of the camera parameters and can be used to efficiently control the motion of nonholonomic mobile robots with an arbitrarily placed and truly unknown overhead camera. Experimental results show that the proposed scheme can achieve satisfactory trajectory tracking control performance despite the lack of any knowledge about the camera intrinsic and extrinsic parameters and the presence of unknown camera lens distortions, and hence, can provide a simple but efficient solution to the vision-based motion control problem of nonholonomic mobile robots.**

***Index Terms*— Calibration free, camera-parameter-independent, fixed camera, image-based control, trajectory tracking.**

I. Introduction

DUE to their many potential applications, localization [1], [2], motion planning [3], [4], motion control [5], target tracking [6], and formation control [7], [8] of mobile robots have been active research topics in the past two decades. To increase the motion control flexibility and accuracy, visual servoing has been extensively used for the feedback control of mobile robots [9]–[15] since its beginning. To establish a visual servo control system for a mobile robot, two camera configurations, eye-in-hand and eye-to-hand configurations, can be adopted according to different application requirements. In the eye-in-hand configuration, the camera is mounted on the mobile robot and will move together with the motion of the mobile robot. In the eye-to-hand configuration, the camera is placed above the robot workspace and can provide a global view of the environment. Up to now, various visual servoing approaches, such as the *position-based visual servoing* (PBVS) (using 3-D pose information provided by some pose estimation algorithms [16], [17]) [18]–[21], *image-based visual servoing* (IBVS) (via the use of 2-D image features) [22]–[26], and *hybrid visual servoing* (HVS) (based on a combination of 2-D image features and 3-D pose information) [27]–[29] have been proposed to deal with the stabilization and tracking control problems of nonholonomic mobile robots.

It should be pointed out that the PBVS approaches not only rely on metrical information of the 3-D scene geometry but also require perfect knowledge of the camera intrinsic parameters. Though the HVS approaches can remove dependence on metrical information of the 3-D scene geometry, they still need

Manuscript received December 11, 2018; revised June 10, 2019 and September 5, 2019; accepted October 28, 2019. Date of publication December 4, 2019; date of current version April 7, 2020. This article was recommended for publication by Associate Editor W. Sheng and Editor K. Saitou upon evaluation of the reviewers' comments. This work was supported in part by the Natural Science Foundation of China under Grant 61673272, Grant U1813219, Grant U1613218, and Grant 61722309; in part by the Beijing Advanced Innovation Center for Intelligent Robots and Systems under Grant 2019IRS01; and in part by the Fundamental Research Funds for the Central Universities under Grant 16X100040016. *(Corresponding author: Hesheng Wang.)*

X. Liang is with the School of Aeronautics and Astronautics, Shanghai Jiao Tong University, Shanghai 200240, China (e-mail: xinwu113@163.com).

H. Wang is with the Department of Automation, Key Laboratory of System Control and Information Processing of Ministry of Education, Key Laboratory of Marine Intelligent Equipment and System of Ministry of Education, Shanghai Jiao Tong University, Shanghai 200240, China, and also with the Beijing Advanced Innovation Center for Intelligent Robots and Systems, Beijing Institute of Technology, Beijing 100081, China (e-mail: wanghesheng@sjtu.edu.cn).

Y.-H. Liu and Z. Liu are with the Department of Mechanical and Automation Engineering, The Chinese University of Hong Kong, Hong Kong (e-mail: yhliu@mae.cuhk.edu.hk; zheliu@cuhk.edu.hk).

B. You is with the Maintenance Department III, Fujian Fuqing Nuclear Power Co., Ltd., Fuqing 350300, China (e-mail: youbing01@cnnp.com.cn).

W. Chen is with the Department of Automation, Shanghai Jiao Tong University, Shanghai 200240, China (e-mail: wdchen@sjtu.edu.cn).

Color versions of one or more of the figures in this article are available online at http://ieeexplore.ieee.org.

Digital Object Identifier 10.1109/TASE.2019.2951714

to know the accurate values of the camera intrinsic parameters. In the PBVS or HVS approaches, the control accuracy can be largely affected by errors in the camera intrinsic parameters, and to obtain higher performance, an offline precise calibration of the camera intrinsic parameters is necessary. It is known that the approaches depending on offline precise parameter identification are not robust to disturbances and changes of the parameters. As an attractive feature, the IBVS approaches have better robustness against calibration errors of the camera parameters, and errors in some reasonable ranges can be allowed without affecting the control accuracy. When the calibration errors are too large, and beyond the tolerable ranges, however, the robot closed-loop system may become unstable, and the approximate values of the camera parameters are required to ensure closed-loop stability. For this reason, an offline coarse calibration of the camera parameters is a prerequisite for many of the previously mentioned IBVS approaches.

It is worth noting that there have been some IBVS approaches proposed for the control of mobile robots, which are known as the uncalibrated IBVS approaches and do not impose bound constraints on the errors of the camera parameters, such as the approaches in [30]–[33]. To deal with uncertainties in the camera parameters, an adaptive tracking controller was proposed in [30] for the eye-to-hand configuration. The stabilization problem of mobile robots with uncertainties in the camera parameters was addressed in [31]. The image plane is required to be parallel to the motion plane in the articles [30] and [31]. Though the parallelism requirement between the image and motion planes was removed in [26], partial camera intrinsic and extrinsic parameters were assumed to be known. In our previous articles [32], [33], IBVS controllers without the parallelism requirement were proposed to compensate for uncertainties in the camera intrinsic and extrinsic parameters.

Theoretically, arbitrarily large errors in the camera parameters will not cause instability of the closed-loop system in the above-mentioned uncalibrated IBVS approaches [30]–[33]. Such high robustness with respect to the camera parameter errors is achieved by designing adaptive laws to compensate for the parameter uncertainties, and an online adaptive calibration of the camera parameters is performed in these IBVS approaches. The online adaptive calibration can enhance system robustness to errors and changes in the parameters, but to obtain satisfactory control performance, rough estimates of the camera parameters that are not too far from their true values should be used in the controller design. The use of too rough estimates may deteriorate the transient performance of the closed-loop system, or in the worst case, may lead to system instability in real applications. Then, an offline coarse camera calibration (or, a rough guess) is still necessary for these uncalibrated IBVS approaches. Note that in [34], an approach without any calibration of the camera parameters was proposed to solve the metrology problem, but not the control problem as addressed in our current work. It should be pointed out that many uncalibrated visual servoing approaches have been proposed for the control of robotic manipulators, such as the approaches in [35]–[49]. Offline camera calibration can be avoided in these uncalibrated visual servoing approaches, but online camera calibration, which is performed by the use of adaptive laws [35]–[44] or numerical estimation algorithms [45]–[49], is needed. Hence, the truly uncalibrated vision-based control of mobile robots that can be implemented without any offline or online calibration of the camera parameters is still an open problem, which is very desirable to be solved for easier implementation and enhanced system robustness.

The controller proposed in our previous article [50] can be designed without any knowledge of the camera intrinsic and extrinsic parameters and can be used to guide the mobile robot to the desired position from an initial position, but cannot drive the mobile robot along the desired trajectory. In real applications, it is very important to control the mobile robot to move along a desired trajectory to a desired position, in order to achieve obstacle avoidance or keep the mobile robot in the camera field of view during the control process, either of which is known to be the key to success of task execution. In this article, we propose a novel scheme for the trajectory tracking control of mobile robots with an overhead fixed camera. The proposed control scheme can be applied without any offline or online calibration of the camera intrinsic and extrinsic parameters and belongs to a truly uncalibrated IBVS approach. Due to the camera-calibration-free nature, the proposed scheme makes it possible to use a completely unknown camera for the tracking control tasks without any precise or coarse knowledge of its intrinsic and extrinsic parameters. Note that our previous work in [50] aims to deal with the position control problem, while the current work in this article is to address the trajectory tracking control problem. Hence, the proposed control scheme in the current work is different from that in our previous article [50], and is the first one that can handle the trajectory tracking control problem of nonholonomic mobile robots without any offline or online camera calibration. The main contributions of this article can be summarized as: 1) a visual servo trajectory tracking controller with a depth-ratio-based image Jacobian matrix is proposed. The proposed controller can be considered as an extension of the position controller in our previous article [50], and hence, the use of the depth-ratio-based image Jacobian matrix can allow the camera to be mounted overhead with an arbitrary pose, without knowing its intrinsic and extrinsic parameters. Note that the controller developed in our previous article [50] can only deal with the position stabilization problem, which is a very special case of the trajectory tracking problem addressed by the proposed controller in this article. 2) Compared with our previous article [50], improved methods for the online estimation of the depth ratios according to their dynamics are presented. Furthermore, some improvements in the calculation of the Jacobian matrix, based on rough values of the feature depths, are also given in the current work. 3) The robustness analysis of the proposed controller with respect to estimation errors of the depth ratios is provided. 4) The stability of the closed-loop control system in the presence of the camera lens distortion is analyzed. 5) Experimental results are provided to validate the proposed trajectory tracking control scheme. In our previous articles [32], [33] and many other existing uncalibrated visual servoing approaches, the offline precise calibration of

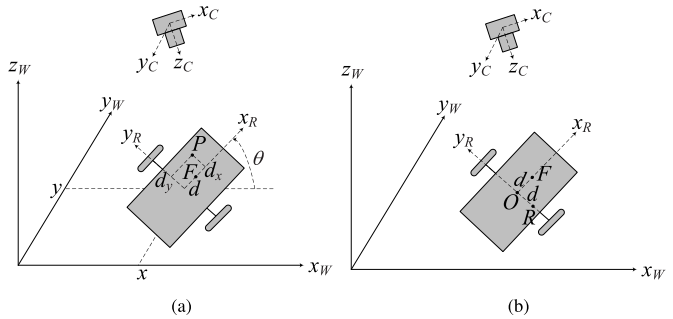

Fig. 1. System setup. (a) Mobile robot system with an overhead camera. (b) System setup for the proposed image-based kinematic model.

the camera parameters is not necessary, but online adaptive camera calibration, which requires an offline coarse calibration or approximate guess of the camera parameters to improve the control performance, is still desired. With this in mind, the novelty of the proposed scheme lies in the fact that both online and offline camera calibration can be totally eliminated, and no knowledge of the camera parameters is necessary such that the trajectory tracking controller design for the mobile robots can be largely simplified, which could be very appealing from the point of view of users.

II. Problem Formulation

A. Perspective Projection Model

In this article, we consider the vision-based trajectory tracking control of nonholonomic mobile robots with an overhead fixed camera. The mobile robot is driven by two independently controlled rear wheels, and the robot system with a fixed camera is shown in Fig. 1(a). The camera used for the control tasks is assumed to be a pinhole camera and is placed above the working area of the mobile robot. Assume that during the robot motion, feature points attached to the mobile robot can always be detected by the camera and can be continuously tracked by the visual tracking system. As shown in Fig. 1(a), three coordinate frames are defined to describe the robot motion, including the world coordinate frame W, the robot coordinate frame R, and the camera coordinate frame C. The origin of the coordinate frame R is located at the geometric center of the robot, and the x-axis is perpendicular to the axis of rear wheels and points in the forward direction of the robot, while the y-axis is along the axis of rear wheels and points toward the left-hand side of the robot. According to the right-hand rule, the z-axis of the coordinate frame R can be defined. The homogeneous transformation matrix from the coordinate frame W to the coordinate frame C is denoted by $\mathbf{T}_W^C \in \mathbb{R}^{4\times4}$ [$\mathbf{R}_W^C \in SO(3)$ and $\boldsymbol{t}_W^C \in \mathbb{R}^{3\times1}$ are, respectively, its rotational and translational components], which encodes the camera extrinsic parameters. For a fixed camera, the camera extrinsic parameters are constant. Under the planar motion assumption, the position of the mobile robot on the motion plane is represented by $\boldsymbol{x} = (x, y)^\top \in \mathbb{R}^{2\times1}$, and the orientation is defined as the angle θ between the x-axis of the coordinate frame W and the x-axis of the coordinate frame R, as shown in Fig. 1(a).

Assume that a general feature point P is attached on the mobile robot as shown in Fig. 1(a), and its 3-D homogeneous coordinates with respect to the coordinate frame R is given by $\boldsymbol{x}_p^R = (\boldsymbol{d}_p^\top, 0, 1)^\top \in \mathbb{R}^{4\times1}$, where $\boldsymbol{d}_p = (d_x, d_y)^\top \in \mathbb{R}^{2\times1}$ is the planar local coordinates of the feature point P with respect to the coordinate frame R. The 3-D homogeneous coordinates of the feature point P with respect to the coordinate frame W can be expressed as $\boldsymbol{x}_p^W = (\boldsymbol{x}_p^\top, 0, 1)^\top \in \mathbb{R}^{4\times1}$, where $\boldsymbol{x}_p \in \mathbb{R}^{2\times1}$ denotes the planar global coordinates of the feature point P with respect to the coordinate frame W

$$\boldsymbol{x}_p = \boldsymbol{x} + (d_x \cos\theta - d_y \sin\theta, d_x \sin\theta + d_y \cos\theta)^\top. \tag{1}$$

The 3-D homogeneous coordinates of the feature point P with respect to the coordinate frame C can be derived by $\boldsymbol{x}_p^C = \mathbf{T}_W^C \boldsymbol{x}_p^W \in \mathbb{R}^{4\times1}$.

Denote image coordinates of the feature point P on the image plane by $\boldsymbol{y}_p = (u_p, v_p)^\top \in \mathbb{R}^{2\times1}$. Using the perspective projection model of the pinhole camera, we have

$$\begin{bmatrix} \boldsymbol{y}_p \\ 1 \end{bmatrix} = \frac{1}{z_p^C} \boldsymbol{\Omega} \boldsymbol{x}_p^C \tag{2}$$

where $\boldsymbol{\Omega} \in \mathbb{R}^{3\times4}$ is determined by the camera intrinsic parameters $\boldsymbol{\Omega} = [\mathbf{A}\ \mathbf{0}]$, with $\mathbf{A} \in \mathbb{R}^{3\times3}$ being the camera intrinsic matrix, and z_p^C denotes the depth of the feature point P with respect to the coordinate frame C. Substituting the expression of $\boldsymbol{x}_p^C$ into (2) yields

$$\begin{bmatrix} \boldsymbol{y}_p \\ 1 \end{bmatrix} = \frac{1}{z_p^C} \mathbf{A} \begin{bmatrix} \boldsymbol{r}_1 & \boldsymbol{r}_2 & \boldsymbol{t}_W^C \end{bmatrix} \tilde{\boldsymbol{x}}_p \triangleq \frac{1}{z_p^C} \mathbf{H} \tilde{\boldsymbol{x}}_p \tag{3}$$

where $\boldsymbol{r}_i \in \mathbb{R}^{3\times1}$ denotes the ith column of the rotation matrix $\mathbf{R}_W^C$, $\tilde{\boldsymbol{x}}_p = (\boldsymbol{x}_p^\top, 1)^\top \in \mathbb{R}^{3\times1}$ is the 2-D homogeneous coordinates of the feature point P with respect to the world coordinate frame, and $\mathbf{H} \in \mathbb{R}^{3\times3}$ represents the homography matrix between the image and motion planes and depends on the camera intrinsic and extrinsic parameters. Based on (3), we can obtain the compact expressions of image coordinates of the feature point P and its depth

$$z_p^C = \boldsymbol{h}_3^\top \tilde{\boldsymbol{x}}_p, \quad \boldsymbol{y}_p = \frac{1}{z_p^C} \begin{bmatrix} \boldsymbol{h}_1^\top \\ \boldsymbol{h}_2^\top \end{bmatrix} \tilde{\boldsymbol{x}}_p \tag{4}$$

where $\boldsymbol{h}_i^\top \in \mathbb{R}^{1\times3}$ is the ith row vector of the matrix $\mathbf{H}$.

B. Image-Based Kinematics Model

The kinematics of nonholonomic mobile robots can be written as

$$\dot{x} = v \cos\theta, \quad \dot{y} = v \sin\theta, \ \dot{\theta} = \omega \tag{5}$$

where v and ω, respectively, represent the linear and angular velocities of the mobile robot and are control inputs to be designed for the trajectory tracking control of the mobile robot.

Differentiating $\tilde{\boldsymbol{x}}_p$ with respect to time results in

$$\dot{\tilde{\boldsymbol{x}}}_p = \begin{bmatrix} \cos\theta & -d_x \sin\theta - d_y \cos\theta \\ \sin\theta & d_x \cos\theta - d_y \sin\theta \\ 0 & 0 \end{bmatrix} \begin{bmatrix} v \\ \omega \end{bmatrix} \triangleq \mathbf{D}_p \begin{bmatrix} v \\ \omega \end{bmatrix} \tag{6}$$

where $\mathbf{D}_p \in \mathbb{R}^{3\times 2}$ and the kinematic model (5) has been used. Differentiating the second equation of (4) with respect to time, and then substituting the time derivative of the depth z_p^C, we can easily have

$$\dot{\boldsymbol{y}}_p = \frac{1}{z_p^C}\begin{bmatrix} \boldsymbol{h}_1^\top - u_p \boldsymbol{h}_3^\top \\ \boldsymbol{h}_2^\top - v_p \boldsymbol{h}_3^\top \end{bmatrix} \dot{\tilde{\boldsymbol{x}}}_p \triangleq \frac{1}{z_p^C}\mathbf{L}_p \dot{\tilde{\boldsymbol{x}}}_p \tag{7}$$

where $\mathbf{L}_p \in \mathbb{R}^{2\times 3}$ is the depth-independent interaction matrix. Finally, substituting (6) into (7), we can obtain the kinematic model of the mobile robot on the image plane for the case when the general feature point P is used to describe the position of the mobile robot

$$\dot{\boldsymbol{y}}_p = \frac{1}{z_p^C}\mathbf{L}_p\mathbf{D}_p\begin{bmatrix} v \\ \omega \end{bmatrix} \triangleq \frac{1}{z_p^C}\mathbf{Q}_p\begin{bmatrix} v \\ \omega \end{bmatrix} \tag{8}$$

where $\mathbf{Q}_p \in \mathbb{R}^{2\times 2}$ is known as the depth-independent image Jacobian matrix of the mobile robot associated with the general feature point P.

C. Problem Statement

When an overhead camera is used for a vision-based control task, image position of one onboard feature point is sufficient to describe the robot position on the motion plane, and if this feature point can be controlled to move along a desired trajectory on the image plane, the mobile robot can be ensured to track an equivalent desired trajectory on the motion plane. To achieve the trajectory tracking control objective, we use a particular feature point located at the forward axis of the mobile robot as such a feature point, i.e., the feature point F, as shown in Fig. 1(a). Then, the image position of the feature point F, i.e., image coordinates $\boldsymbol{y}_f = (u_f, v_f)^\top \in \mathbb{R}^{2\times 1}$, can define the robot position on the motion plane, and the trajectory tracking control objective can be achieved by controlling the image position $\boldsymbol{y}_f$ to track its desired image trajectory defined by $\boldsymbol{y}_{fd} \in \mathbb{R}^{2\times 1}$.

Problem 1: Given a desired trajectory of the feature point F, which is defined by the desired image position $\boldsymbol{y}_{fd}$ and velocity $\dot{\boldsymbol{y}}_{fd}$, design truly uncalibrated (which means that the camera intrinsic and extrinsic parameters do not need to be estimated by using online or offline algorithms) vision-based controllers to provide control inputs (v, ω) for a mobile robot using feedback information from an overhead fixed pinhole camera, without any offline or online calibration of the camera parameters, such that the feature point F can track its desired image trajectory in the sense that the image position tracking errors $\Delta\boldsymbol{y}_f = \boldsymbol{y}_f - \boldsymbol{y}_{fd}$ and the image velocity tracking errors $\Delta\dot{\boldsymbol{y}}_f = \dot{\boldsymbol{y}}_f - \dot{\boldsymbol{y}}_{fd}$ converge to zero as time goes to infinity.

To address *Problem 1*, the key is to establish a relationship between control inputs (v, ω) and the image velocity $\dot{\boldsymbol{y}}_f$, i.e., the image-based kinematics of the mobile robot associated with the feature point F. Based on the perspective projection model for the general feature point P, expressions of image coordinates $\boldsymbol{y}_f$ of the feature point F and its depth z_f^C can be derived by substituting the local coordinates $\boldsymbol{d}_f = (d, 0)^\top \in \mathbb{R}^{2\times 1}$ ($d_x = d$, $d_y = 0$) into (4)

$$z_f^C = \boldsymbol{h}_3^\top \tilde{\boldsymbol{x}}_f, \quad z_f^C u_f = \boldsymbol{h}_1^\top \tilde{\boldsymbol{x}}_f, \; z_f^C v_f = \boldsymbol{h}_2^\top \tilde{\boldsymbol{x}}_f \tag{9}$$

where $\tilde{\boldsymbol{x}}_f = (x + d\cos\theta, y + d\sin\theta, 1)^\top \in \mathbb{R}^{3\times 1}$ is the 2-D homogeneous coordinates of the feature point F with respect to the world coordinate frame. The kinematic model of the mobile robot on the image plane associated with the feature point F can be obtained by substituting the local coordinates $\boldsymbol{d}_f = (d, 0)^\top$ into (8)

$$\dot{\boldsymbol{y}}_f = \frac{1}{z_f^C}\begin{bmatrix} q_{11} & q_{12} \\ q_{21} & q_{22} \end{bmatrix}\begin{bmatrix} v \\ \omega \end{bmatrix} \triangleq \frac{1}{z_f^C}\mathbf{Q}_f\begin{bmatrix} v \\ \omega \end{bmatrix} \tag{10}$$

where $\mathbf{Q}_f \in \mathbb{R}^{2\times 2}$ denotes the depth-independent image Jacobian matrix associated with the feature point F, and

$$\begin{aligned} q_{11} &= h_{11}\cos\theta + h_{12}\sin\theta \\ &\quad - u_f(h_{31}\cos\theta + h_{32}\sin\theta) \end{aligned} \tag{11}$$

$$\begin{aligned} q_{12} &= -h_{11}d\sin\theta + h_{12}d\cos\theta \\ &\quad + u_f(h_{31}d\sin\theta - h_{32}d\cos\theta) \end{aligned} \tag{12}$$

$$\begin{aligned} q_{21} &= h_{21}\cos\theta + h_{22}\sin\theta \\ &\quad - v_f(h_{31}\cos\theta + h_{32}\sin\theta) \end{aligned} \tag{13}$$

$$\begin{aligned} q_{22} &= -h_{21}d\sin\theta + h_{22}d\cos\theta \\ &\quad + v_f(h_{31}d\sin\theta - h_{32}d\cos\theta) \end{aligned} \tag{14}$$

where h_{ij} is the element of the homography matrix $\mathbf{H}$ in the ith row and jth column.

To design a visual servo controller by using the image-based kinematic model (10)–(14), one possible way is to accurately calibrate the camera parameters in an offline manner. To avoid the tedious offline precise calibration of the camera parameters, an alternative way is to develop adaptive controllers by designing estimation laws for online camera calibration, as done in the previous articles [30]–[33]. Though the approaches based on online camera calibration can eliminate dependence on exact knowledge of the camera parameters, coarse knowledge of them is still required. To completely remove dependence on any *a priori* knowledge of the camera parameters, it is necessary to design a truly uncalibrated vision-based trajectory tracking controller without any offline or online camera calibration, which has not been solved by existing approaches and is our main objective in this article. Considering the explicit dependence on the camera parameters, it is impossible to design truly uncalibrated visual servo trajectory tracking controllers via the use of the image-based kinematic model (10)–(14). To solve this problem, new image-based kinematic models have to be derived.

III. Camera-Parameter-Independent Image-Based Kinematic Model

When one can develop image-based kinematic models without depending on the camera parameters, the design of truly uncalibrated visual servo trajectory tracking controllers can become straightforward. To make such design possible, we next present a camera-parameter-independent image-based kinematic model for mobile robots with an overhead camera.

Besides the feature point F, two additional feature points are used to facilitate the development of the proposed kinematic model, i.e., the feature point O, which is located at the origin of the coordinate frame R, and the feature point R, which

is located at the right-hand side of the wheel axis of the mobile robot. The arrangement of the feature points is shown in Fig. 1(b). As seen from Fig. 1(b), the distance between the feature points R and O is equal to that between the feature points F and O, which is the model parameter d.

Based on the perspective projection model for the feature point P, expressions of image coordinates $\boldsymbol{y}_o = (u_o, v_o)^\top \in \mathbb{R}^{2\times 1}$ of the feature point O and its depth z_o^C can be deduced by substituting the local coordinates $\boldsymbol{d}_o = (0,0)^\top \in \mathbb{R}^{2\times 1}$ ($d_x = 0$, $d_y = 0$) into (4)

$$z_o^C = \boldsymbol{h}_3^\top \tilde{\boldsymbol{x}}_o, \quad z_o^C u_o = \boldsymbol{h}_1^\top \tilde{\boldsymbol{x}}_o, \quad z_o^C v_o = \boldsymbol{h}_2^\top \tilde{\boldsymbol{x}}_o \tag{15}$$

where $\tilde{\boldsymbol{x}}_o = (x, y, 1)^\top \in \mathbb{R}^{3\times 1}$ denotes the 2-D homogeneous coordinates of the feature point O with respect to the world coordinate frame. Substituting the local coordinates $\boldsymbol{d}_r = (0, -d)^\top \in \mathbb{R}^{2\times 1}$ ($d_x = 0$, $d_y = -d$) into (4), we can obtain image coordinates $\boldsymbol{y}_r = (u_r, v_r)^\top \in \mathbb{R}^{2\times 1}$ of the feature point R and its depth z_r^C

$$z_r^C = \boldsymbol{h}_3^\top \tilde{\boldsymbol{x}}_r, \quad z_r^C u_r = \boldsymbol{h}_1^\top \tilde{\boldsymbol{x}}_r, \quad z_r^C v_r = \boldsymbol{h}_2^\top \tilde{\boldsymbol{x}}_r \tag{16}$$

where $\tilde{\boldsymbol{x}}_r = (x + d\sin\theta, y - d\cos\theta, 1)^\top \in \mathbb{R}^{3\times 1}$ is the 2-D homogeneous coordinates of the feature point R with respect to the world coordinate frame. The proposed image-based kinematic model can be derived by reformulating the kinematic model (10)–(14) through the use of image information of the three feature points, as detailed in the following.

For convenience, we define $\tilde{\boldsymbol{d}}_f = (d\cos\theta, d\sin\theta, 0)^\top \in \mathbb{R}^{3\times 1}$ and $\tilde{\boldsymbol{d}}_r = (d\sin\theta, -d\cos\theta, 0)^\top \in \mathbb{R}^{3\times 1}$. Then, we have

$$\tilde{\boldsymbol{x}}_f = \tilde{\boldsymbol{x}}_o + \tilde{\boldsymbol{d}}_f \tag{17}$$

$$\tilde{\boldsymbol{x}}_r = \tilde{\boldsymbol{x}}_o + \tilde{\boldsymbol{d}}_r. \tag{18}$$

From (11), we have

$$q_{11} = \frac{1}{d}\left(\boldsymbol{h}_1^\top \tilde{\boldsymbol{d}}_f - u_f \boldsymbol{h}_3^\top \tilde{\boldsymbol{d}}_f\right). \tag{19}$$

Substituting (17) into (19) and then using the first two equations of (9) and the first two equations of (15) gives

$$q_{11} = \frac{1}{d} z_o^C (u_f - u_o). \tag{20}$$

Using the definition $\tilde{\boldsymbol{d}}_r$, (12) can be rewritten as

$$q_{12} = -\boldsymbol{h}_1^\top \tilde{\boldsymbol{d}}_r + u_f \boldsymbol{h}_3^\top \tilde{\boldsymbol{d}}_r. \tag{21}$$

Substituting (18) into (21), then from the first two equations of (15) and the first two equations of (16), we can obtain

$$q_{12} = z_r^C (u_f - u_r) - z_o^C (u_f - u_o). \tag{22}$$

Using the definition $\tilde{\boldsymbol{d}}_f$, (13) can be rewritten as

$$q_{21} = \frac{1}{d}\left(\boldsymbol{h}_2^\top \tilde{\boldsymbol{d}}_f - v_f \boldsymbol{h}_3^\top \tilde{\boldsymbol{d}}_f\right). \tag{23}$$

Substituting (17) into (23) and then applying the first and third equations of (9) and the first and third equations of (15), we can have

$$q_{21} = \frac{1}{d} z_o^C (v_f - v_o). \tag{24}$$

Based on the definition $\tilde{\boldsymbol{d}}_r$, (14) can be reexpressed as

$$q_{22} = -\boldsymbol{h}_2^\top \tilde{\boldsymbol{d}}_r + v_f \boldsymbol{h}_3^\top \tilde{\boldsymbol{d}}_r. \tag{25}$$

Substituting (18) into (25), then through the use of the first and third equations of (15) and the first and third equations of (16), we have

$$q_{22} = z_r^C (v_f - v_r) - z_o^C (v_f - v_o). \tag{26}$$

Now, we have obtained the camera-parameter-independent image-based kinematic model as follows:

$$\dot{\boldsymbol{y}}_f = \frac{1}{z_f^C} \mathbf{Q}_f \begin{bmatrix} \nu \\ \omega \end{bmatrix} \triangleq \mathbf{J}_f \begin{bmatrix} \nu \\ \omega \end{bmatrix} \tag{27}$$

where $\mathbf{J}_f \in \mathbb{R}^{2\times 2}$ is called the overall image Jacobian matrix

$$\mathbf{J}_f = \frac{1}{z_f^C} \begin{bmatrix} \frac{1}{d} z_o^C (u_f - u_o) & z_r^C (u_f - u_r) - z_o^C (u_f - u_o) \\ \frac{1}{d} z_o^C (v_f - v_o) & z_r^C (v_f - v_r) - z_o^C (v_f - v_o) \end{bmatrix}$$

from which we can see that the camera intrinsic and extrinsic parameters can be completely removed from the image-based kinematic model by introducing two additional particular feature points. The proposed camera-parameter-independent image-based kinematic model can be fully characterized by image information of the three feature points and their depths, and can pave the way for the design of controllers without any offline or online camera calibration.

Before going into the trajectory tracking controller design, some facts about the relationship between projections of the feature points on the image plane are given in the following propositions. Denote projected points of the feature points F, R, and O on the image plane by f, r, and o, respectively.

Proposition 1: Any two of projected points f, r, and o are never located at the same position on the image plane.

Proposition 2: Projected points f, r, and o will never be collinear on the image plane.

Considering that *Propositions 1* and *2* can be easily proved by contradiction, we omit their proofs here. As a direct consequence from *Propositions 1* and *2*, we can directly have the following proposition.

Proposition 3: Projected points f, r, and o always form a nondegenerate triangle (i.e., a triangle with nonzero area).

IV. Depth-Ratio-Based Trajectory Tracking Control Scheme

In this section, we present the trajectory tracking controller design to address *Problem 1*, without imposing any constraint on the mounting pose of the overhead camera. Note that the image-based kinematic model (27) can be reformulated into a nice form by rearranging terms

$$\dot{\boldsymbol{y}}_f = \begin{bmatrix} \frac{1}{d}\alpha_{of}(u_f - u_o) & \alpha_{rf}(u_f - u_r) - \alpha_{of}(u_f - u_o) \\ \frac{1}{d}\alpha_{of}(v_f - v_o) & \alpha_{rf}(v_f - v_r) - \alpha_{of}(v_f - v_o) \end{bmatrix} \begin{bmatrix} \nu \\ \omega \end{bmatrix} \triangleq \mathbf{J}_{f\alpha} \begin{bmatrix} \nu \\ \omega \end{bmatrix} \tag{28}$$

where $\mathbf{J}_{f\alpha} \in \mathbb{R}^{2\times 2}$ is called the depth-ratio-based image Jacobian matrix, and $\alpha_{of} = z_o^C/z_f^C$ and $\alpha_{rf} = z_r^C/z_f^C$ denote the depth ratios between the feature points. As we know, without integrating the use of other sensors, it is difficult to directly measure the depth information from images of a single camera in the absence of exact knowledge about the camera, which is known as one of the main causes of difficulties in the design of visual servo controllers using traditional image-based kinematic models. Due to the camera-parameter-independent feature of the proposed kinematic model, in the following proposition, we show that the depth ratios can be directly computed by using image information of three feature points and motion information of the mobile robot despite the lack of knowledge about the camera.

Proposition 4: The depth ratios α_{of} and α_{rf} can be measured based on the optical flow technique if the motion of the mobile robot satisfies the following conditions:

$$\omega \neq 0, \quad \nu \neq d\omega. \tag{29}$$

Proof: By rearranging the terms, (28) can be easily reformulated as

$$\begin{aligned}\dot{\boldsymbol{y}}_f &= \begin{bmatrix} \{\frac{\nu}{d} - \omega\}(u_f - u_o) & \omega(u_f - u_r) \\ \{\frac{\nu}{d} - \omega\}(v_f - v_o) & \omega(v_f - v_r) \end{bmatrix} \begin{bmatrix} \alpha_{of} \\ \alpha_{rf} \end{bmatrix} \\ &\triangleq \mathbf{M}_\alpha \begin{bmatrix} \alpha_{of} \\ \alpha_{rf} \end{bmatrix}. \end{aligned} \tag{30}$$

The determinant of $\mathbf{M}_\alpha$ can be determined as $\det \mathbf{M}_\alpha = \{(\nu/d) - \omega\}\omega \det[\overrightarrow{of} \ \ \overrightarrow{rf}]$. According to *Proposition 3*, we have $\det[\overrightarrow{of} \ \ \overrightarrow{rf}] \neq 0$. Then, if the robot motion satisfies the conditions in (29), we have $\det \mathbf{M}_\alpha \neq 0$. From the expression of $\mathbf{M}_\alpha$, we know that $\mathbf{M}_\alpha$ can be calculated through the use of image information of the feature points and motion information of the mobile robot (which can be obtained using wheel encoders). Hence, by using the optical flow technique, the depth ratios can be measured by

$$\begin{bmatrix} \alpha_{of} \\ \alpha_{rf} \end{bmatrix} = \mathbf{M}_\alpha^{-1} \dot{\boldsymbol{y}}_f \tag{31}$$

where $\dot{\boldsymbol{y}}_f$ is the optical flow of the feature point F. ■

Remark 1: Based on the conditions in (29), we can know that to provide excitation for the measurement of the depth ratios using (31), initial movements of the mobile robot with pure rotations (i.e., $\nu = 0$ and $\omega \neq 0$) are sufficient. The conditions given here for the static estimation of the depth ratios are very similar to those provided in [21] for the dynamic estimation of the mobile robot pose, which can be considered as the persistent excitation conditions [51] particularly for the case of noniterative parameter estimation.

Remark 2: To make the mobile robot track a time-varying desired image trajectory $\boldsymbol{y}_{fd}$ satisfying $\dot{\boldsymbol{y}}_{fd} \neq 0$, it is impossible for the robot motion to satisfy the conditions $\omega = 0$ and $\nu = 0$ except at the initial instant before starting the tracking. As stated in *Remark 1*, the measurability problem at the initial conditions $\omega = 0$ and $\nu = 0$ can be overcome by performing an open-loop initial movement with a pure rotation. At some instants, when the robot motion does not satisfy the conditions in (29), the depth ratio α_{of} or α_{rf} cannot be measured. One possible solution to this issue is to use the most recent measurements of the depth ratios for the controller design at the time when they cannot be reliably measured by the optical flow technique.

Actually, to deal with the measurability problem that may be encountered at the time when the depth ratios cannot be directly/reliably measured, an alternative slightly complex solution is to estimate the depth ratios based on their previous measurements and the robot motion information, according to the dynamics of the depth ratios.

Proposition 5: If the robot motion at the current time satisfies the following conditions:

$$\omega = 0, \quad \nu \neq 0 \tag{32}$$

the depth ratios α_{of} and α_{rf} at the current time can be estimated by

$$\alpha_{of,k} = \frac{d\|\dot{\boldsymbol{y}}_{f,k}\|}{|\nu_k|\|\boldsymbol{y}_{f,k} - \boldsymbol{y}_{o,k}\|} \tag{33}$$

$$\alpha_{rf,k} = \alpha_{rf,k-1} + \frac{\tau}{d}\nu_{k-1}(1 - \alpha_{of,k-1})(1 - \alpha_{rf,k-1}) \tag{34}$$

where the subscripts $k-1$ and k, respectively, denote the previous and the current time indexes, and τ represents the sampling time.

Proof: When $\omega = 0$ and $\nu \neq 0$, (30) can be expressed as

$$\dot{\boldsymbol{y}}_f = \frac{\nu}{d}(\boldsymbol{y}_f - \boldsymbol{y}_o)\alpha_{of}. \tag{35}$$

Taking the norm of both sides of (35) results in $\|\dot{\boldsymbol{y}}_f\| = |\nu|/d\|\boldsymbol{y}_f - \boldsymbol{y}_o\|\alpha_{of}$, from which (33) can be directly obtained since we have $\|\boldsymbol{y}_f - \boldsymbol{y}_o\| \neq 0$ according to *Proposition 3*. Differentiating the first equation of (16) with respect to time and then using (17) and the first equations of (9) and (15), we can readily have

$$\dot{z}_r^C = \left\{\frac{\nu}{d} + \omega\right\}\left(z_f^C - z_o^C\right). \tag{36}$$

Furthermore, differentiating the first equation of (9) with respect to time and then applying (17), (18), and the first equations of (9), (15), and (16), we can finally obtain

$$\dot{z}_f^C = \frac{\nu}{d}\left(z_f^C - z_o^C\right) - \omega\left(z_r^C - z_o^C\right). \tag{37}$$

Based on the use of (36) and (37), the time derivative $\dot{\alpha}_{rf}$ can be derived as

$$\dot{\alpha}_{rf} = \frac{\nu}{d}(1-\alpha_{of})(1-\alpha_{rf}) + \omega(1-\alpha_{of}) + \omega\alpha_{rf}(\alpha_{rf}-\alpha_{of}). \tag{38}$$

Hence, if $\omega = 0$ and $\nu \neq 0$, from (38), we have $\dot{\alpha}_{rf} = \nu/d(1-\alpha_{of})(1-\alpha_{rf})$, which arrives at (34) by using the forward difference approximation to $\dot{\alpha}_{rf,k-1}$. ■

Proposition 6: If the robot motion at the current time does not satisfy either of the conditions in (29) or (32), the depth

ratios α_{of} and α_{rf} at the current time can be estimated by

$$\begin{aligned}\alpha_{of,k} &= \alpha_{of,k-1} + \tau\left\{\left[\frac{\nu_{k-1}}{d}-\omega_{k-1}\right]\alpha_{of,k-1}^2+\left[\omega_{k-1}\alpha_{rf,k-1}-\frac{2\nu_{k-1}}{d}\right]\times\alpha_{of,k-1}+\frac{\nu_{k-1}}{d}\right\} \quad (39)\\ \alpha_{rf,k} &= \alpha_{rf,k-1}+\tau\left\{(1-\alpha_{of,k-1})\left[\frac{\nu_{k-1}}{d}(1-\alpha_{rf,k-1})+\omega_{k-1}\right]+\omega_{k-1}\alpha_{rf,k-1}(\alpha_{rf,k-1}-\alpha_{of,k-1})\right\}. \quad (40)\end{aligned}$$

Proof: Differentiating the first equation of (15) with respect to time and then using (17) and the first equations of (9) and (15) yields

$$\dot{z}_o^C = \frac{\nu}{d}\left(z_f^C - z_o^C\right). \quad (41)$$

Then, based on (37) and (41), the time derivative of the depth ratio α_{of} can be derived as

$$\dot{\alpha}_{of} = \left\{\frac{\nu}{d}-\omega\right\}\alpha_{of}^2+\left\{\omega\alpha_{rf}-\frac{2\nu}{d}\right\}\alpha_{of}+\frac{\nu}{d} \quad (42)$$

which leads to (39) by using the forward difference approximation to $\dot{\alpha}_{of,k-1}$. Similarly, applying the forward difference approximation to $\dot{\alpha}_{rf,k-1}$ in (38) directly results in (40). ■

Remark 3: It is noted that the conditions in *Proposition 4* mean that the mobile robot undergoes a pure rotational motion without translation or a combined translational and rotational motion such that the velocity vector $\boldsymbol{v}_f$ of the feature point F on the motion plane is not parallel to the feature vector $\overrightarrow{RF}$, while those in *Proposition 5* indicate that the mobile robot moves with a pure translational motion. Then, the conditions in *Proposition 6* equivalently say that the mobile robot is motionless or performs a combined translational and rotational motion such that the velocity vector $\boldsymbol{v}_f$ is parallel to the feature vector $\overrightarrow{RF}$.

Since the depth ratios can be measured using the optical flow technique, $\mathbf{J}_{f\alpha}$ can easily be calculated based on the integrated use of the image information and the robot motion information without any offline/online camera calibration. When $\mathbf{J}_{f\alpha}$ is nonsingular, we can use its inverse to design tracking controllers to solve *Problem 1*.

Proposition 7: The depth-ratio-based image Jacobian matrix $\mathbf{J}_{f\alpha}$ is always nonsingular.

Proof: By using simple calculations, we can obtain $\det\mathbf{J}_{f\alpha} = (1/d)\alpha_{of}\alpha_{rf}\det[\overrightarrow{of}\ \overrightarrow{rf}]$, from which we directly have $\det\mathbf{J}_{f\alpha}\neq 0$ since $\det[\overrightarrow{of}\ \overrightarrow{rf}]\neq 0$ and the depth ratios α_{of} and α_{rf} are always positive. ■

Considering that the image Jacobian matrix $\mathbf{J}_{f\alpha}$ is nonsingular, its inverse $\mathbf{J}_{f\alpha}^{-1}$ can be used to design the trajectory tracking controller

$$\begin{bmatrix}\nu\\ \omega\end{bmatrix} = \mathbf{J}_{f\alpha}^{-1}(\dot{\boldsymbol{y}}_{fd}-\mathbf{K}_{f\alpha}\Delta\boldsymbol{y}_f) \quad (43)$$

where $\mathbf{K}_{f\alpha}\in\mathbb{R}^{2\times 2}$ is a symmetric positive definite matrix. Note that the controller (43) is designed for *the ideal case* when exact values of the depth ratios can be available. *In the perturbed case* when only estimated depth ratios $\hat{\alpha}_{of}$ and $\hat{\alpha}_{rf}$ can be used, the trajectory tracking controller needs to be developed by using the estimated depth-ratio-based image Jacobian matrix $\hat{\mathbf{J}}_{f\alpha}$ (which is obtained by replacing the depth ratios of $\mathbf{J}_{f\alpha}$ with their estimated values), and can be designed in the same form as the controller (43)

$$\begin{bmatrix}\nu\\ \omega\end{bmatrix} = \hat{\mathbf{J}}_{f\alpha}^{-1}(\dot{\boldsymbol{y}}_{fd}-\mathbf{K}_{f\alpha}\Delta\boldsymbol{y}_f). \quad (44)$$

Now, we present the main result in this article as follows.

Theorem 1: Assume that the overhead fixed camera is a pinhole camera and mounted at an arbitrary pose, and some metric information from the mobile robot is available (i.e., the model parameter d is exactly known). *In the ideal case* when exact values of the depth ratios can be available, the controller (43) guarantees that the mobile robot can track the desired trajectory defined by the desired image trajectory of the feature point F, i.e., the image position and velocity tracking errors $\Delta\boldsymbol{y}_f$ and $\Delta\dot{\boldsymbol{y}}_f$ converge to zero exponentially as time goes to infinity. *In the perturbed case* when only estimated depth ratios can be used, the controller (44) ensures that the image position and velocity tracking errors are globally uniformly ultimately bounded for any positive estimated depth ratios if the desired image trajectory is given such that $\lim_{t\to\infty}\dot{\boldsymbol{y}}_{fd}\neq 0$.

Proof: In the ideal case, we can obtain the closed-loop system dynamics by substituting (43) into (28)

$$\Delta\dot{\boldsymbol{y}}_f = -\mathbf{K}_{f\alpha}\Delta\boldsymbol{y}_f \quad (45)$$

which directly shows the exponential convergence of the image position and velocity tracking errors $\Delta\boldsymbol{y}_f$ and $\Delta\dot{\boldsymbol{y}}_f$ *in the ideal case*.

In the perturbed case, substituting (44) into (28) results in the closed-loop system dynamics

$$\Delta\dot{\boldsymbol{y}}_f = -\mathbf{J}_{f\alpha}\hat{\mathbf{J}}_{f\alpha}^{-1}\mathbf{K}_{f\alpha}\Delta\boldsymbol{y}_f+\left(\mathbf{J}_{f\alpha}\hat{\mathbf{J}}_{f\alpha}^{-1}-\mathbf{I}_2\right)\dot{\boldsymbol{y}}_{fd}. \quad (46)$$

By expanding the expression of $\mathbf{J}_{f\alpha}\hat{\mathbf{J}}_{f\alpha}^{-1}$, it is not difficult to conclude that when the estimated depth ratios satisfy the following conditions:

$$\frac{\alpha_{of}}{\hat{\alpha}_{of}}+\frac{\alpha_{rf}}{\hat{\alpha}_{rf}}>0,\quad \frac{\alpha_{of}}{\hat{\alpha}_{of}}\frac{\alpha_{rf}}{\hat{\alpha}_{rf}}>0 \quad (47)$$

the matrix $-\mathbf{J}_{f\alpha}\hat{\mathbf{J}}_{f\alpha}^{-1}\mathbf{K}_{f\alpha}$ is guaranteed to be a Hurwitz matrix. Then according to the theory for time-varying linear systems with a nonvanishing perturbation [52], we know that once the conditions in (47) are met, globally uniformly ultimately boundedness (GUUB) of the tracking errors can be achieved when the desired image trajectory is given such that $\lim_{t\to\infty}\dot{\boldsymbol{y}}_{fd}\neq 0$. Considering that the conditions in (47) are true if $\hat{\alpha}_{of}>0$ and $\hat{\alpha}_{rf}>0$, *in the perturbed case*, GUUB of the tracking errors is guaranteed by any positive estimated depth ratios, but theoretically, to obtain better tracking control performance, more accurate estimated values of the depth ratios should be used for the controller design as can be seen from the second term of (46). Furthermore, from (46), we can also conclude that *in the perturbed case*, if the desired image trajectory is defined such that $\lim_{t\to\infty}\dot{\boldsymbol{y}}_{fd}=0$, asymptotical

convergence of the tracking errors can be ensured by any positive estimated depth ratios. ■

Remark 4: In the implementation of the trajectory tracking controller (43), the use of closed-form inverse of the image Jacobian matrix $\mathbf{J}_{f\alpha}$ is a better choice in comparison with the numerical inverse, considering that the calculation of closed-form inverse of a 2×2 matrix is very straightforward and can be faster.

Remark 5: When some *a priori* knowledge about the camera extrinsic parameters (such as the camera installation height and angle) is readily available, rough values of the feature depths can be obtained. In this case, the proposed camera-calibration-free trajectory tracking controller can be implemented in a simpler way by using the depth-based image Jacobian matrix $\mathbf{J}_f$ (which can be estimated via the use of fixed rough values of the feature depths) but not the depth-ratio-based image Jacobian matrix $\mathbf{J}_{f\alpha}$ (which is calculated from online estimated values of the depth ratios), i.e., we have

$$\begin{bmatrix} v \\ \omega \end{bmatrix} = \mathbf{J}_f^{-1}(\dot{\boldsymbol{y}}_{fd} - \mathbf{K}_{f\alpha}\Delta \boldsymbol{y}_f). \tag{48}$$

As will be shown by the experimental results in Section V, the proposed controller using the estimated depth-based image Jacobian matrix can also achieve satisfactory control performance, and hence, in practical applications, can be considered as an alternative solution to the camera-calibration-free trajectory tracking control problem of nonholonomic mobile robots.

Remark 6: The dependence on the optical flow technique can be considered as a drawback of the propose trajectory tracking controller using the depth-ratio-based image Jacobian matrix. Note that measurements of the depth ratios based on the optical flow technique can introduce some complexities into the controller design, since the image velocity information and the motion information of the mobile robot are needed besides the image position information of the feature points, and some techniques are required to properly handle the potential problems induced by the use of the optical flow. Keeping this in mind, the proposed camera-calibration-free trajectory tracking controller based on the optical flow technique still needs to be further improved by designing new depth-ratio estimation methods without image velocity measurements in future research.

Remark 7: In the presence of camera lens distortion, only distorted image coordinates $\breve{\boldsymbol{y}}_i = (\breve{u}_i, \breve{v}_i)^\top \in \mathbb{R}^{2\times 1}$ $(i = f, r, o)$ of the feature points can be used for controller design. Hence, the controller (43) in this case is implemented as the following form:

$$\begin{bmatrix} v \\ \omega \end{bmatrix} = \breve{\mathbf{J}}_{f\alpha}^{-1}(\dot{\boldsymbol{y}}_{fd} - \mathbf{K}_{f\alpha}\Delta \breve{\boldsymbol{y}}_f) \tag{49}$$

where $\breve{\mathbf{J}}_{f\alpha}$ is obtained by replacing the undistorted image coordinates $\boldsymbol{y}_i$ of $\mathbf{J}_{f\alpha}$ with the distorted one $\breve{\boldsymbol{y}}_i$, and $\Delta\breve{\boldsymbol{y}}_f = \breve{\boldsymbol{y}}_f - \boldsymbol{y}_{fd}$. Note that $\breve{\boldsymbol{y}}_i$ can be related to $\boldsymbol{y}_i$ by $\breve{\boldsymbol{y}}_i = \boldsymbol{y}_i + \boldsymbol{\delta}_i$, where $\boldsymbol{\delta}_i = (\delta_{iu}, \delta_{iv})^\top \in \mathbb{R}^{2\times 1}$, and δ_{iu} and δ_{iv} are, respectively, used to denote the nonlinear functions $\delta_u(u_i, v_i)$ and $\delta_v(u_i, v_i)$, which model the nonlinear lens distortion effects. Taking the time derivative of $\breve{\boldsymbol{y}}_f$ yields $\dot{\breve{\boldsymbol{y}}}_f = \dot{\boldsymbol{y}}_f + \dot{\boldsymbol{\delta}}_f$, and then substituting (28) and $\boldsymbol{y}_i = \breve{\boldsymbol{y}}_i - \boldsymbol{\delta}_i$ finally leads to

$$\dot{\breve{\boldsymbol{y}}}_f = \breve{\mathbf{J}}_{f\alpha}\begin{bmatrix} v \\ \omega \end{bmatrix} + \boldsymbol{\gamma}_f \tag{50}$$

where $\boldsymbol{\gamma}_f \in \mathbb{R}^{2\times 1}$ denotes a perturbation term induced by the camera lens distortion and is defined by $\boldsymbol{\gamma}_f = [\alpha_{of}/d(\boldsymbol{\delta}_o - \boldsymbol{\delta}_f)\ \alpha_{rf}(\boldsymbol{\delta}_r - \boldsymbol{\delta}_f) - \alpha_{of}(\boldsymbol{\delta}_o - \boldsymbol{\delta}_f)](v, \omega)^\top + \dot{\boldsymbol{\delta}}_f$. Substituting (49) into (50), we obtain the closed-loop dynamics in the presence of camera lens distortion

$$\Delta\dot{\breve{\boldsymbol{y}}}_f = -\mathbf{K}_{f\alpha}\Delta\breve{\boldsymbol{y}}_f + \boldsymbol{\gamma}_f. \tag{51}$$

It is noted that the nominal system of (51) is exponentially stable, and there exist two positive constants γ_1 and γ_2 such that the perturbation term $\boldsymbol{\gamma}_f$ can be bounded by $\|\boldsymbol{\gamma}_f\| \le \gamma_1\|\Delta\breve{\boldsymbol{y}}_f\| + \gamma_2$. Then, based on the results for exponentially stable systems with a nonvanishing perturbation [52], we conclude that GUUB of the tracking errors $\Delta\breve{\boldsymbol{y}}_f$ can be guaranteed in the presence of camera lens distortion.

Remark 8: Though the control developments in this article are based on the planar motion assumption, from an implementation point of view, the proposed trajectory tracking controller using the depth-ratio-based image Jacobian matrix is still applicable in the situations when the mobile robot moves on nonplanar surfaces. In such situations, depth values of the feature points may change suddenly with a large amplitude, but usually, the depth ratios still change with very small amplitude. Most importantly, the values of the depth ratios can be measured based on the optical flow technique in a real-time manner. Theoretical robustness analysis of the proposed trajectory tracking controller with respect to nonplanar motion is an interesting research topic but is extremely difficult due to the challenge in the derivation of a useful analytical expression to represent the kinematics of the mobile robot running on general nonplanar surfaces.

Remark 9: As shown in the proposed image-based kinematics model, the image Jacobian matrix directly depends on the model parameter d. Though considerable deviation errors of this parameter from its true value can be tolerated by the proposed trajectory tracking controller, a good estimate is needed to obtain satisfactory tracking control performance. Hence, some *a priori* knowledge about the model parameter d is still required for the controller design. Nevertheless, as compared with the tediousness and difficulty in the calibration of the camera intrinsic and extrinsic parameters, *a priori* knowledge requirement of the model parameter does not introduce much trouble into the implementation of the proposed trajectory tracking controller, since it can be directly measured with guaranteed accuracy by just using a common ruler.

Remark 10: It should be pointed out that in the proposed trajectory tracking controller, the feature marker plane is assumed to be completely parallel to the motion plane. Such parallelism condition is required to guarantee that these two planes can be equivalently treated as the same plane to obtain a very simple and elegant camera-parameter-independent image-based kinematics model. However, it may be difficult to make the feature marker plane strictly parallel to the motion plane due to potential alignment errors in real applications. Hence, the extension of the proposed controller to a more general case

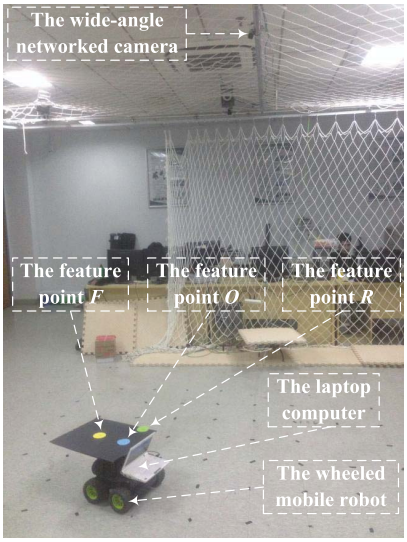

Fig. 2. Experimental system setup.

when the parallelism condition is not a satisfied or theoretical analysis of its robustness with respect to the orientation offset error between these two planes is interesting. But to that end, some very challenging issues still need to be addressed.

V. Experimental Results

In this section, experimental results based on a mobile robot platform are presented to demonstrate the feasibility and effectiveness of the proposed trajectory tracking controller. The experimental system setup is shown in Fig. 2. In this setup, a wide-angle networked camera is fixed overhead to perform the motion detection task for the mobile robot. To make image processing easier and to enhance the robustness of feature extraction and tracking, three colored circular markers have been attached on the mobile robot. As shown in Fig. 2, geometric centers of the yellow, green, and blue circular markers are, respectively, taken as feature points F, R, and O, and the model parameter d is about 0.18 m. Note that in our study, we find that the model parameter d is not necessary to be known precisely. Actually, the proposed trajectory tracking controller still can achieve satisfactory tracking control performance even when the model parameter used in the controller design deviates from its true value with a 30% error, which shows good robustness of the proposed trajectory tracking controller with respect to the errors of the model parameter d. However, when the deviation error becomes much larger, the tracking control performance can be deteriorated. This implies that to obtain satisfactory tracking control performance, some *a priori* knowledge about the model parameter d is still required for the controller design.

By using the cable network, images from the wide-angle networked camera are transmitted to the host computer. After receiving images from the camera, the image processing system running on the host computer will continuously extract and track the feature points, whose image positions will be forwarded to the laptop computer using the wireless network. Based on the received image positions of the feature points, the proposed tracking control scheme executed on the laptop computer can calculate the control inputs and then send them to the embedded system onboard the mobile robot via a USB port. Once the control commands from the laptop computer have been received, the low-level controller running on the embedded system will generate corresponding driving signals for the wheels to drive the mobile robot to move along its desired trajectory defined by the desired image trajectory of the feature point F. The previous processes form a feedback loop and execute repeatedly at a frequency of about 20 Hz for continuous tracking of the desired trajectory.

In the implementation, the optical flow of the feature point F is obtained based on the filtered differentiation of the measured image position of the feature point F, which is continuously provided by the marker-based feature detection and tracking algorithm. In addition, the robot velocities are estimated based on the relationship between the robot velocities and the wheel velocities, i.e., $v = (\omega_r + \omega_l)/2r$ and $\omega = (\omega_r - \omega_l)/br$, where b is the width of the mobile robot, r represents the wheel radius, and ω_r and ω_l, respectively, denote the angular velocities of the right and left driving wheels and are obtained from numerical differentiation of the angles of the right and left driving wheels measured by the wheel encoders. Note that the depth ratios are estimated based on the combined use of the methods in *Propositions 4–6*. Specifically, the depth ratios are obtained using the method in *Proposition 4* if the robot motion satisfies the conditions in (29), otherwise, they are computed by applying the methods in *Propositions 5* and *6*.

To illustrate the performance of the proposed trajectory tracking controller using the depth-ratio-based image Jacobian matrix $\mathbf{J}_{f\alpha}$ (*Controller (43)*, which is formally stated in *Theorem 1*), two groups of experiments have been conducted, respectively, for two kinds of desired image trajectories, i.e., the desired circular image trajectory and the desired figure-eight image trajectory. Furthermore, for each group, two types of experiments have been performed, respectively, under two conditions on the placement of the camera, i.e., *the parallel condition* under which the optical axis is made to be perpendicular to the ground plane, and *the unparallel condition* under which the angle between the optical axis and the vertical line is made to be about 20°. Note that to clearly show the effects that the radial lens distortion can have in the system performance, comparison results between two cases, *the undistorted case* when the undistorted image coordinates of the feature points are used for the controller design and *the distorted case* when the distorted image coordinates of the feature points are directly employed, have been obtained for each condition of each group. In the implementation, we do not carry out any offline calibration of the camera parameters to obtain their precise or coarse values. Moreover, we do not perform any online adaptive calibration of the camera parameters to estimate their values for the controller design. In other words, both offline and online camera calibration can be avoided, and no knowledge of the camera is needed in the implementation of *Controller (43)*. For all the experiments, the controller gain $\mathbf{K}_{f\alpha} = 0.8\mathbf{I}_2$ is used.

In the first group of experiments, the desired trajectory of the mobile robot is specified by the desired circular

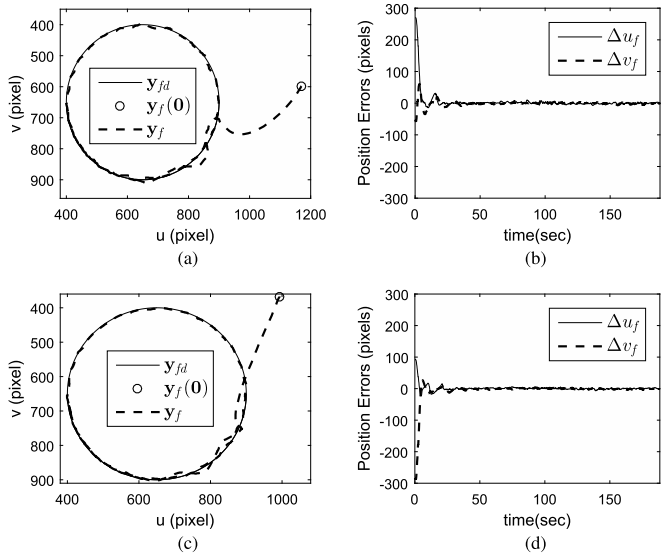

Fig. 3. Experimental results for *Controller (43)* and the desired circular image trajectory under the parallel condition [***the undistorted case:*** (a) and (b); ***the distorted case:*** (c) and (d)]. (a) and (c) Desired and real image trajectories. (b) and (d) Image position tracking errors.

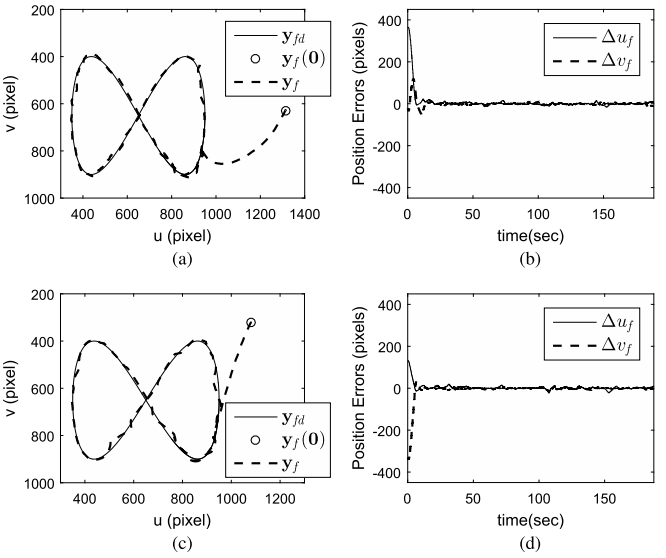

Fig. 5. Experimental results for *Controller (43)* and the desired figure-eight image trajectory under the parallel condition [***the undistorted case:*** (a) and (b); ***the distorted case:*** (c) and (d)]. (a) and (c) Desired and real image trajectories. (b) and (d) Image position tracking errors.

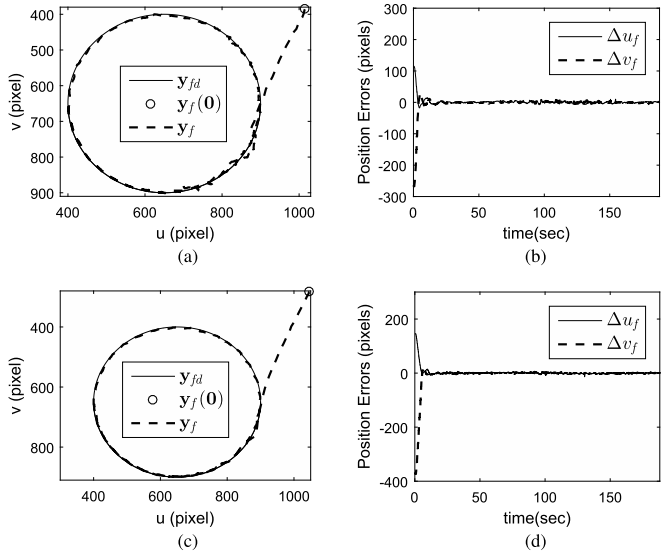

Fig. 4. Experimental results for *Controller (43)* and the desired circular image trajectory under the unparallel condition [***the undistorted case:*** (a) and (b); ***the distorted case:*** (c) and (d)]. (a) and (c) Desired and real image trajectories. (b) and (d) Image position tracking errors.

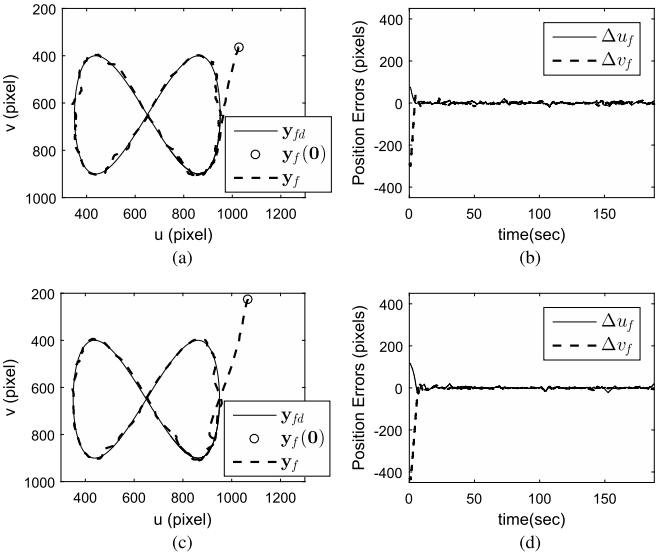

Fig. 6. Experimental results for *Controller (43)* and the desired figure-eight image trajectory under the unparallel condition [***the undistorted case:*** (a) and (b); ***the distorted case:*** (c) and (d)]. (a) and (c) Desired and real image trajectories. (b) and (d) Image position tracking errors.

image trajectory of the feature point F, $\boldsymbol{y}_{fd} = (650 + 250\cos(0.05\ t), 650 + 250\sin(0.05\ t))^\top$ pixels. Under the parallel condition, experimental results are given in Fig. 3, from which we observe that the mobile robot can well track its desired trajectory, and the convergence of the image position tracking errors can be guaranteed. This confirms the conclusion of *Theorem 1* and also shows that the radial lens distortion does not have an obvious negative effect on the system performance of the proposed controller. Under the unparallel condition, experimental results are shown in Fig. 4, from which we find that good tracking of the desired trajectory and convergence of the image position tracking errors can still be ensured by *Controller (43)*, which shows the effectiveness of *Controller (43)* in dealing with the truly uncalibrated trajectory tracking control problem and further demonstrates its good robustness with respect to the radial lens distortion.

In the second group of experiments, the mobile robot is required to move along a more complex trajectory defined by the desired figure-eight image trajectory of the feature point F, $\boldsymbol{y}_{fd} = (650 + 300\cos(0.04t), 650 + 250\sin(0.08t))^\top$ pixels. In this setting, experimental results under the parallel condition are shown in Fig. 5, while experimental results under the unparallel condition are given in Fig. 6. From Figs. 5 and 6, we see that under both conditions, the mobile robot can track the desired trajectory satisfactorily in both the undistorted and the distorted cases, which further confirms the effectiveness

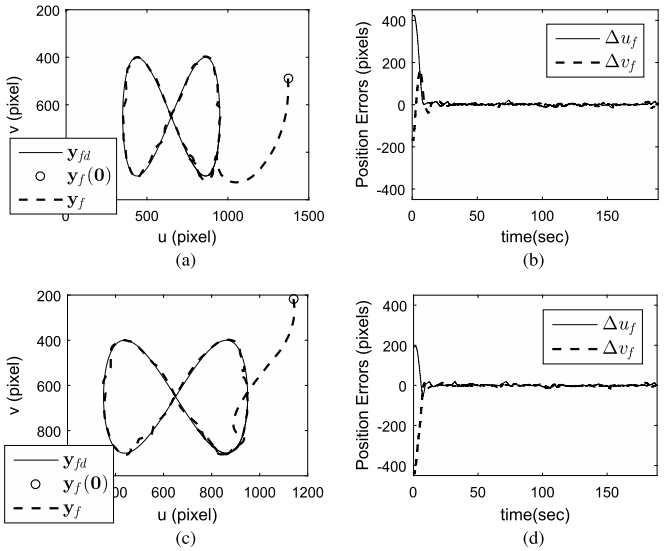

Fig. 7. Experimental results for *Controller (43)* and the desired figure-eight image trajectory in the presence of the orientation offset error between the motion and feature marker planes, under the unparallel condition [***the undistorted case:*** (a) and (b); ***the distorted case:*** (c) and (d)]. (a) and (c) Desired and real image trajectories. (b) and (d) Image position tracking errors.

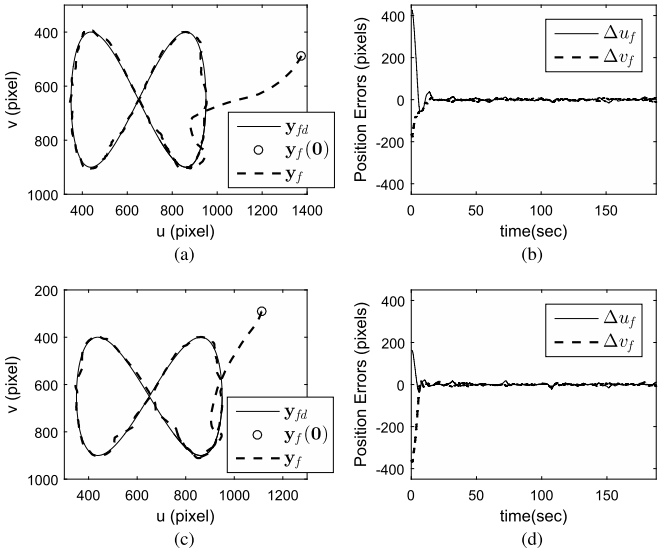

Fig. 8. Experimental results for *Controller (48)* and the desired figure-eight image trajectory under the unparallel condition [***the undistorted case:*** (a) and (b); ***the distorted case:*** (c) and (d)]. (a) and (c) Desired and real image trajectories. (b) and (d) Image position tracking errors.

of *Controller (43)* and shows its good robustness against the radial lens distortion.

To demonstrate the robustness of the proposed trajectory tracking controller using the depth-ratio-based image Jacobian matrix $\mathbf{J}_{f\alpha}$ [i.e., *Controller (43)*] with respect to the orientation offset between the motion and feature marker planes, experiments have been carried out in the case when the motion and feature marker planes are not parallel to each other. In these experiments, the angle between these two planes is set to about 14°, and the same desired figure-eight image trajectory as described earlier needs to be tracked by the mobile robot. Under the unparallel condition, corresponding experimental results are provided in Fig. 7, from which we can see that though there exists a considerable orientation offset between these two planes, satisfactory convergence of the image tracking errors can still be ensured by the proposed *Controller (43)*. Note that the control performance of the proposed *Controller (43)* under the parallel condition is similar to that shown in Fig. 7, and hence, corresponding experimental results are not given here. These results show that the proposed *Controller (43)* can guarantee sufficient robustness with respect to the orientation offset error such that it can be implemented easily in real applications without putting much effort into the installation of the feature marker plane.

To show the performance of the proposed trajectory tracking controller using the depth-based image Jacobian matrix $\mathbf{J}_f$ (*Controller (48)*, which is discussed in *Remark 4*), experiments have been conducted for the case when fixed rough values of the feature depths are used for controller design. In the experiments, the objective is to control the mobile robot to track the same desired figure-eight image trajectory as earlier, and corresponding experimental results under the unparallel condition are given in Fig. 8. From Fig. 8, we observe that satisfactory control performance can be guaranteed by *Controller (48)*, which implies that in real applications, it is enough to use fixed rough values of the feature depths to design the trajectory tracking controller based on the camera-parameter-independent image Jacobian matrix in the form of $\mathbf{J}_f$. Moreover, it can be found that the control performance in the distorted case is almost the same as that in the undistorted case, which also proves that the proposed camera-calibration-free trajectory tracking controller is robust in the presence of camera lens distortions.

Finally, experiments have also been performed to illustrate the robustness of the proposed trajectory tracking controller using the depth-based image Jacobian matrix $\mathbf{J}_f$ [i.e., *Controller (48)*] with respect to the orientation offset between the motion and feature marker planes. In these experiments, the same figure-eight image trajectory is taken as the desired trajectory of the mobile robot. In the presence of orientation offset error between these two planes (i.e., 14°), corresponding experimental results under the unparallel condition are presented in Fig. 9. From Fig. 9, it can be seen that satisfactory control performance can still be obtained by the proposed *Controller (48)*. As compared with Fig. 8, it can be found that the control performance in the case when there exists a considerable orientation offset error between the motion and feature marker planes is almost the same as that in the case when the feature marker plane is set to be parallel to the motion plane. This implies good robustness of the proposed *Controller (48)* with respect to the orientation offset error between the motion and feature marker planes. Meanwhile, the experimental results in Fig. 9 further show the robustness of the proposed *Controller (48)* against the camera lens distortions.

Remark 11: Comparison results under different conditions have been provided in this section to demonstrate the performance and robustness of the proposed method. To fully show

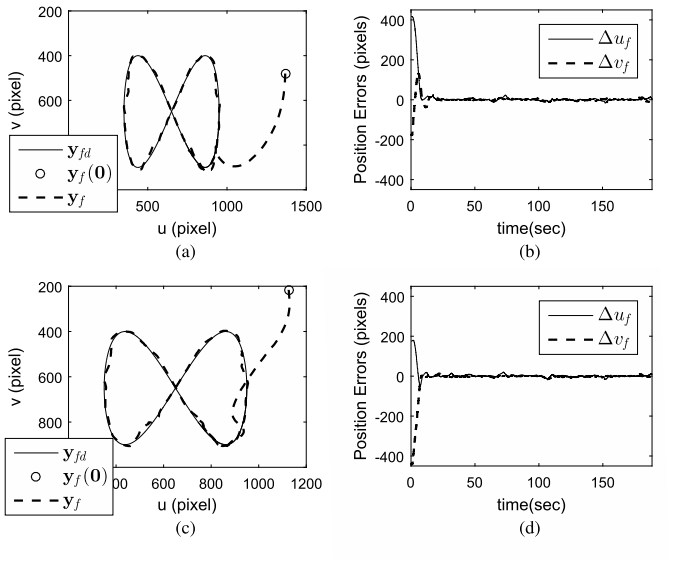

Fig. 9. Experimental results for *Controller (48)* and the desired figure-eight image trajectory in the presence of the orientation offset error between the motion and feature marker planes, under the unparallel condition [***the undistorted case:*** (a) and (b); ***the distorted case:*** (c) and (d)]. (a) and (c) Desired and real image trajectories. (b) and (d) Image position tracking errors.

the superior performance and value of the proposed method, it is necessary to provide some comparison results with other methods if they can be used to solve the same control problem. The thing is that, for other existing uncalibrated image-based trajectory tracking control methods, offline precise calibration of the camera intrinsic and extrinsic parameters is not needed, but online adaptive camera calibration, which requires an offline coarse calibration or approximate guess of the camera parameters to improve the control performance, is desired. In contrast, the proposed image-based trajectory tracking control method in this article can completely eliminate both online and offline camera calibration and does not depend on any knowledge of the camera intrinsic and extrinsic parameters. Hence, the problem solved by the proposed method is totally different from those addressed by other existing methods. To the best of our knowledge, the proposed method is the first one that can solve the camera-calibration-free trajectory tracking control problem of mobile robots without any knowledge of the camera intrinsic and extrinsic parameters, and as we know, in the literature, there has been no other method to address the same control problem.

VI. Conclusion

In this article, we proposed a novel calibration-free image-based trajectory tracking control scheme for mobile robots with an overhead fixed camera. The proposed scheme guarantees that the mobile robot can track the desired image trajectory without any offline or online calibration of the camera intrinsic and extrinsic parameters and no knowledge about the camera is required for its implementation. It is shown that exponential convergence of the image position and velocity tracking errors can be guaranteed by the proposed scheme. Finally, experimental results based on a mobile robot platform were given to illustrate the performance of the proposed scheme. Note that the parallelism between the motion and feature marker planes is necessary for the development of the proposed calibration-free image-based trajectory tracking control scheme. Hence, our future research objective is to study the possibility of extending the proposed scheme to the case without such parallelism requirement. As an alternative, theoretical analysis of the robustness of the proposed scheme with respect to the orientation offset error between the motion and feature marker planes is also one of our future research topics. Considering the necessity of exact knowledge about the model parameter in the design of the proposed scheme, calibration-free trajectory tracking control in the presence of model parameter uncertainty is another important but challenging research direction and deserves to be investigated to further improve the control system performance/robustness and increase the controller design flexibility.

Acknowledgment

The authors would like to thank the associate editor and the anonymous reviewers for their valuable comments and helpful suggestions to improve the quality of this article.

References

[1] H. Cheng, H. Chen, and Y. Liu, "Topological indoor localization and navigation for autonomous mobile robot," *IEEE Trans. Autom. Sci. Eng.*, vol. 12, no. 2, pp. 729–738, Apr. 2015.

[2] F.-A. Moreno, D. Zuñiga-Noël, D. Scaramuzza, and J. Gonzalez-Jimenez, "PL-SLAM: A stereo SLAM system through the combination of points and line segments," *IEEE Trans. Robot.*, vol. 35, no. 3, pp. 734–746, Jun. 2019.

[3] W. Chi, C. Wang, J. Wang, and M. Q.-H. Meng, "Risk-DTRRT-based optimal motion planning algorithm for mobile robots," *IEEE Trans. Autom. Sci. Eng.*, vol. 16, no. 3, pp. 1271–1288, Jul. 2019, doi: 10.1109/TASE.2018.2877963.

[4] X. Zhang, J. Wang, Y. Fang, and J. Yuan, "Multilevel humanlike motion planning for mobile robots in complex indoor environments," *IEEE Trans. Autom. Sci. Eng.*, vol. 16, no. 3, pp. 1244–1258, Jul. 2019, doi: 10.1109/TASE.2018.2880245.

[5] Z. Song, H. Ren, J. Zhang, and S. S. Ge, "Kinematic analysis and motion control of wheeled mobile robots in cylindrical workspaces," *IEEE Trans. Autom. Sci. Eng.*, vol. 13, no. 2, pp. 1207–1214, Apr. 2016.

[6] E. Benli, Y. Motai, and J. Rogers, "Human behavior-based target tracking with an omni-directional thermal camera," *IEEE Trans. Cogn. Develop. Syst.*, vol. 11, no. 1, pp. 36–50, Mar. 2019.

[7] X. Liang, Y.-H. Liu, H. Wang, W. Chen, K. Xing, and T. Liu, "Leader-following formation tracking control of mobile robots without direct position measurements," *IEEE Trans. Autom. Control*, vol. 61, no. 12, pp. 4131–4137, Dec. 2016.

[8] X. Liang, H. Wang, Y.-H. Liu, W. Chen, and T. Liu, "Formation control of nonholonomic mobile robots without position and velocity measurements," *IEEE Trans. Robot.*, vol. 34, no. 2, pp. 434–446, Apr. 2018.

[9] P. Murrieri, D. Fontanelli, and A. Bicchi, "A hybrid-control approach to the parking problem of a wheeled vehicle using limited view-angle visual feedback," *Int. J. Robot. Res.*, vol. 23, nos. 4–5, pp. 437–448, 2004.

[10] G. Chesi, G. L. Mariottini, D. Prattichizzo, and A. Vicino, "Epipole-based visual servoing for mobile robots," *Adv. Robot.*, vol. 20, no. 2, pp. 255–280, 2006.

[11] N. R. Gans and S. A. Hutchinson, "A stable vision-based control scheme for nonholonomic vehicles to keep a landmark in the field of view," in *Proc. IEEE Int. Conf. Robot. Automat.*, Roma, Italy, Apr. 2007, pp. 2196–2201.

[12] S. Bhattacharya, R. Murrieta-Cid, and S. Hutchinson, "Optimal paths for landmark-based navigation by differential-drive vehicles with field-of-view constraints," *IEEE Trans. Robot.*, vol. 23, no. 1, pp. 47–59, Feb. 2007.

[13] G. López-Nicolás, C. Sagüés, J. J. Guerrero, D. Kragic, and P. Jensfelt, "Switching visual control based on epipoles for mobile robots," *Robot. Auton. Syst.*, vol. 56, no. 7, pp. 592–603, Jul. 2008.

[14] H. M. Becerra, J. B. Hayet, and C. Sagüés, "A single visual-servo controller of mobile robots with super-twisting control," *Robot. Auton. Syst.*, vol. 62, no. 11, pp. 1623–1635, Nov. 2014.

[15] J. Chen, B. Jia, and K. Zhang, "Trifocal tensor-based adaptive visual trajectory tracking control of mobile robots," *IEEE Trans. Cybern.*, vol. 47, no. 11, pp. 3784–3798, Nov. 2017.

[16] A. K. Das, R. Fierro, V. Kumar, B. Southall, J. Spletzer, and C. J. Taylor, "Real-time vision-based control of a nonholonomic mobile robot," in *Proc. IEEE Int. Conf. Robot. Automat.*, Seoul, South Korea, May 2001, pp. 1714–1719.

[17] L. Kneip, D. Scaramuzza, and R. Siegwart, "A novel parametrization of the perspective-three-point problem for a direct computation of absolute camera position and orientation," in *Proc. IEEE Int. Conf. Comput. Vis. Pattern Recognit.*, Colorado Springs, CO, USA, Jun. 2011, pp. 2969–2976.

[18] Y. Fang, W. E. Dixon, D. M. Dawson, and P. Chawda, "Homography-based visual servo regulation of mobile robots," *IEEE Trans. Syst., Man, Cybern. B, Cybern.*, vol. 35, no. 5, pp. 1041–1050, Oct. 2005.

[19] J. Chen, W. E. Dixon, M. Dawson, and M. McIntyre, "Homography-based visual servo tracking control of a wheeled mobile robot," *IEEE Trans. Robot.*, vol. 22, no. 2, pp. 407–416, Apr. 2006.

[20] S. S. Mehtatt, W. E. Dixon, D. Mac Arthur, and C. D. Crane, "Visual servo control of an unmanned ground vehicle via a moving airborne monocular camera," in *Proc. Amer. Control Conf.*, Minneapolis, MN, USA, Jun. 2006, pp. 5276–5281.

[21] H. M. Becerra and C. Sagüés, "Exploiting the trifocal tensor in dynamic pose estimation for visual control," *IEEE Trans. Control Syst. Technol.*, vol. 21, no. 5, pp. 1931–1939, Sep. 2013.

[22] G. L. Mariottini, G. Oriolo, and D. Prattichizzo, "Image-based visual servoing for nonholonomic mobile robots using epipolar geometry," *IEEE Trans. Robot.*, vol. 23, no. 1, pp. 87–100, Feb. 2007.

[23] G. López-Nicolás, N. R. Gans, S. Bhattacharya, C. Sagüés, J. J. Guerrero, and S. Hutchinson, "Homography-based control scheme for mobile robots with nonholonomic and field-of-view constraints," *IEEE Trans. Syst., Man, Cybern. B, Cybern.*, vol. 40, no. 4, pp. 1115–1127, Aug. 2010.

[24] H. M. Becerra, G. López-Nicolás, and C. Sagüés, "A sliding-mode-control law for mobile robots based on epipolar visual servoing from three views," *IEEE Trans. Robot.*, vol. 27, no. 1, pp. 175–183, Feb. 2011.

[25] H. Aliakbarpour, O. Tahri, and H. Araujo, "Visual servoing of mobile robots using non-central catadioptric cameras," *Robot. Auton. Syst.*, vol. 62, pp. 1613–1622, Nov. 2014.

[26] R. Kelly, E. Bugarin, and V. Sanchez, "Image-based visual control of nonholonomic mobile robots via velocity fields: Case of partially calibrated inclined camera," in *Proc. IEEE Int. Conf. Decis. Control*, San Diego, CA, USA, Dec. 2006, pp. 3071–3076.

[27] Y. Wang, H. Lang, and C. W. D. Silva, "A hybrid visual servo controller for robust grasping by wheeled mobile robots," *IEEE/ASME Trans. Mechatron.*, vol. 15, no. 5, pp. 757–769, Oct. 2010.

[28] X. Zhang, Y. Fang, and X. Liu, "Motion-estimation-based visual servoing of nonholonomic mobile robots," *IEEE Trans. Robot.*, vol. 27, no. 6, pp. 1167–1175, Dec. 2011.

[29] B. Li, Y. Fang, G. Hu, and X. Zhang, "Model-free unified tracking and regulation visual servoing of wheeled mobile robots," *IEEE Trans. Control Syst. Technol.*, vol. 24, no. 4, pp. 1328–1339, Jul. 2016.

[30] W. E. Dixon, D. M. Dawson, E. Zergeroglu, and A. Behal, "Adaptive tracking control of a wheeled mobile robot via an uncalibrated camera system," *IEEE Trans. Syst., Man, Cybern. B, Cybern.*, vol. 31, no. 3, pp. 341–352, Jun. 2001.

[31] F. Yang and C.-L. Wang, "Adaptive stabilization for uncertain nonholonomic dynamic mobile robots based on visual servoing feedback," *Acta Autom. Sinica*, vol. 37, no. 7, pp. 857–864, Jul. 2011.

[32] X. Liang, H. Wang, and W. Chen, "Adaptive image-based visual servoing of wheeled mobile robots with fixed camera configuration," in *Proc. IEEE Int. Conf. Robot. Automat.*, Hong Kong, May/Jun. 2014, pp. 6199–6204.

[33] X. Liang, H. Wang, W. Chen, D. Guo, and T. Liu, "Adaptive image-based trajectory tracking control of wheeled mobile robots with an uncalibrated fixed camera," *IEEE Trans. Control Syst. Technol.*, vol. 23, no. 6, pp. 2266–2282, Nov. 2015.

[34] A. Criminisi, I. Reid, and A. Zisserman, "Single view metrology," *Int. J. Comput. Vis.*, vol. 40, no. 2, pp. 123–148, 2000.

[35] Y.-H. Liu, H. Wang, C. Wang, and K. K. Lam, "Uncalibrated visual servoing of robots using a depth-independent interaction matrix," *IEEE Trans. Robot.*, vol. 22, no. 4, pp. 804–817, Aug. 2006.

[36] C. Liu, C. C. Cheah, and J. J. E. Slotine, "Adaptive Jacobian tracking control of rigid-link electrically driven robots based on visual task-space information," *Automatica*, vol. 42, no. 9, pp. 1491–1501, 2006.

[37] H. Wang, Y.-H. Liu, and D. Zhou, "Dynamic visual tracking for manipulators using an uncalibrated fixed camera," *IEEE Trans. Robot.*, vol. 23, no. 3, pp. 610–617, Jun. 2007.

[38] H. Wang, Y. H. Liu, and D. Zhou, "Adaptive visual servoing using point and line features with an uncalibrated eye-in-hand camera," *IEEE Trans. Robot.*, vol. 24, no. 4, pp. 843–857, Aug. 2008.

[39] C. C. Cheah, C. Liu, and J. J. E. Slotine, "Adaptive Jacobian vision based control for robots with uncertain depth information," *Automatica*, vol. 46, no. 7, pp. 1228–1233, 2010.

[40] G. Hu, W. MacKunis, N. Gans, W. E. Dixon, J. Chen, A. Behal, and D. Dawson, "Homography-based visual servo control with imperfect camera calibration," *IEEE Trans. Autom. Control*, vol. 54, no. 6, pp. 1318–1324, Jun. 2009.

[41] G. Hu, N. Gans, N. Fitz-Coy, and W. Dixon, "Adaptive homography-based visual servo tracking control via a quaternion formulation," *IEEE Trans. Control Syst. Technol.*, vol. 18, no. 1, pp. 128–135, Jan. 2010.

[42] G. Hu, N. Gans, and W. Dixon, "Quaternion-based visual servo control in the presence of camera calibration error," *Int. J. Robust Nonlinear Control*, vol. 20, no. 5, pp. 489–503, 2010.

[43] X. Liang, H. Wang, Y. Liu, W. Chen, and J. Zhao, "A unified design method for adaptive visual tracking control of robots with eye-in-hand/fixed camera configuration," *Automatica*, vol. 59, pp. 97–105, Sep. 2015.

[44] F. Xu, H. Wang, J. Wang, K. W. S. Au, and W. Chen, "Underwater dynamic visual servoing for a soft robot arm with online distortion correction," *IEEE/ASME Trans. Mechatron.*, vol. 24, no. 3, pp. 979–989, Jun. 2019.

[45] M. Jagersand, O. Fuentes, and R. Nelson, "Experimental evaluation of uncalibrated visual servoing for precision manipulation," in *Proc. IEEE Int. Conf. Robot. Automat.*, Albuquerque, NM, USA, Apr. 1997, pp. 2874–2880.

[46] A. M. Farahmand, A. Shademan, and M. Jagersand, "Global visual-motor estimation for uncalibrated visual servoing," in *Proc. IEEE Int. Conf. Intell. Robots Syst.*, San Diego, CA, USA, Oct./Nov. 2007, pp. 1969–1974.

[47] A. Shademan, A.-M. Farahmand, and M. Jägersand, "Robust jacobian estimation for uncalibrated visual servoing," in *Proc. IEEE Int. Conf. Robot. Automat.*, Anchorage, AK, USA, May 2010, pp. 5564–5569.

[48] J. A. Piepmeier and H. Lipkin, "Uncalibrated eye-in-hand visual servoing," *Int. J. Robot. Res.*, vol. 22, nos. 10–11, pp. 805–819, 2003.

[49] J. A. Piepmeier, G. V. McMurray, and H. Lipkin, "Uncalibrated dynamic visual servoing," *IEEE Trans. Robot. Autom.*, vol. 20, no. 1, pp. 143–147, Feb. 2004.

[50] X. Liang, H. Wang, Y.-H. Liu, W. Chen, and Z. Jing, "Image-based position control of mobile robots with a completely unknown fixed camera," *IEEE Trans. Autom. Control*, vol. 63, no. 9, pp. 3016–3023, Sep. 2018.

[51] R. Bitmead, "Persistence of excitation conditions and the convergence of adaptive schemes," *IEEE Trans. Inf. Theory*, vol. IT-30, no. 2, pp. 183–191, Mar. 1984.

[52] H. K. Khalil, *Nonlinear Systems*, 3rd ed. Upper Saddle River, NJ, USA: Prentice-Hall, 2002.

Xinwu Liang (M'19) received the B.S. and Ph.D. degrees in control engineering from the Huazhong University of Science and Technology, Wuhan, China, in 2006 and 2011, respectively.

He was a Post-Doctoral Fellow with the Department of Automation, Shanghai Jiao Tong University, Shanghai, China, from 2011 to 2014, and a Post-Doctoral Fellow with the Department of Mechanical and Automation Engineering, The Chinese University of Hong Kong, Hong Kong, from 2014 to 2015. He is currently an Associate Professor with the School of Aeronautics and Astronautics, Shanghai Jiao Tong University. His current research interests include robot control, visual servoing, vision-based navigation, adaptive control, and computer vision.

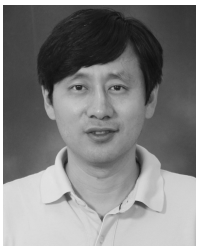

Hesheng Wang (SM'15) received the B.Eng. degree in electrical engineering from the Harbin Institute of Technology, Harbin, China, in 2002, and the M.Phil. and Ph.D. degrees in automation and computer-aided engineering from The Chinese University of Hong Kong, Hong Kong, in 2004 and 2007, respectively.

He was a Post-Doctoral Fellow and Research Assistant with the Department of Mechanical and Automation Engineering, The Chinese University of Hong Kong, from 2007 to 2009. He is currently a Professor with the Department of Automation, Shanghai Jiao Tong University, Shanghai, China. His current research interests include visual servoing, service robot, adaptive robot control, and autonomous driving.

Dr. Wang was the General Chair of the 2016 IEEE International Conference on Real-Time Computing and Robotics and the Program Chair of the 2014 IEEE International Conference on Robotics and Biomimetics and the 2019 IEEE/American Society of Mechanical Engineering International Conference on Advanced Intelligent Mechatronics. He is an Associate Editor of *Assembly Automation*, the *International Journal of Humanoid Robotics*, and the IEEE TRANSACTIONS ON ROBOTICS, and a Technical Editor of the IEEE/ASME TRANSACTIONS ON MECHATRONICS.

Yun-Hui Liu (F'09) received the B.Eng. degree in applied dynamics from the Beijing Institute of Technology, Beijing, China, in 1985, the M.Eng. degree in mechanical engineering from Osaka University, Osaka, Japan, in 1989, and the Ph.D. degree in mathematical engineering and information physics from The University of Tokyo, Tokyo, Japan, in 1992.

He was with the Electrotechnical Laboratory, Ministry of International Trade and Industry, Ibaraki, Japan, from 1992 to 1995. Since 1995, he has been with The Chinese University of Hong Kong (CUHK), Hong Kong, where he is currently a Choh-Ming Li Professor of Mechanical and Automation Engineering and the Director of T Stone Robotics Institute. He is also a Visiting Researcher with the State Key Laboratory of Robotics Technology and System, Harbin Institute of Technology, Harbin, China, and the Director of the Joint Centre for Intelligent Sensing and Systems, National University of Defense Technology, Changsha, China, and CUHK. He has authored or coauthored over 200 articles in refereed journals and refereed conference proceedings. His current research interests include visual servoing, medical robotics, multifingered robot hands, mobile robots, sensor networks, and machine intelligence.

Dr. Liu was a recipient of numerous research awards from international journals and international conferences in robotics and automation and government agencies. He was the General Chair of the 2006 IEEE/RSJ International Conference on Intelligent Robots and Systems. He served as an Associate Editor of the IEEE TRANSACTIONS ON ROBOTICS AND AUTOMATION. He is the Editor-in-Chief of *Robotics and Biomimetics* and an Editor of *Advanced Robotics*. He was listed in the highly cited authors (Engineering) by Thomson Reuters in 2013.

Bing You received the B.S. and M.S. degrees in control engineering from the Huazhong University of Science and Technology, Wuhan, China, in 2006 and 2008, respectively.

He is currently a Senior Control System Engineer with the Maintenance Department III, Fujian Fuqing Nuclear Power Co., Ltd., Fuqing, China. His current research interests include automation control systems, application of robots in nuclear power plants, and cybersecurity of industrial Internet.

Zhe Liu received the B.S. degree in automation from Tianjin University, Tianjin, China, in 2010, and the Ph.D. degree in control technology and control engineering from Shanghai Jiao Tong University, Shanghai, China, in 2016.

He is currently a Post-Doctoral Fellow with the Department of Mechanical and Automation Engineering, The Chinese University of Hong Kong, Hong Kong. His current research interests include autonomous mobile robot, multirobot cooperation, and autonomous driving system.

Weidong Chen (M'04) received the B.S. and M.S. degrees in control engineering and the Ph.D. degree in mechatronics from the Harbin Institute of Technology, Harbin, China, in 1990, 1993, and 1996, respectively.

He was a Visiting Associate Professor with the Department of Electrical and Computer Engineering, The Ohio State University, Columbus, OH, USA, from 2003 to 2004. In 2012, he was a Visiting Professor with the Artificial Intelligence Laboratory, University of Zurich, Zürich, Switzerland. He has been with the Shanghai Jiao Tong University, Shanghai, China, since 1996, where he is currently the Chair and a Professor with the Department of Automation, and the Director of the Institute of Robotics and Intelligent Processing. He is the Founder of the Autonomous Robot Laboratory. His current research interests include autonomous robotics, assistive robotics, collective robotics, and control of mechatronic systems.